Error compensation in Brillouin optical correlation-domain reflectometry by combining bidirectionally measured frequency shift distributions

Guangtao Zhu[1], Kohei Noda[1,2], Heeyoung Lee[3], Kentaro Nakamura[2], and Yosuke Mizuno[1*]

[1] *Faculty of Engineering, Yokohama National University, Yokohama 240-8501, Japan*

[2] *Institute of Innovative Research, Tokyo Institute of Technology, Yokohama 226-8503, Japan*

[3] *College of Engineering, Shibaura Institute of Technology, Tokyo 135-8548, Japan*

[*]E-mail: mizuno-yosuke-rg@ynu.ac.jp

In standard single-end-access Brillouin optical correlation-domain reflectometry (BOCDR), the systematic error caused by the phase difference between amplitude modulation (AM) and frequency modulation (FM) in the light source can be up to tens of megahertz, causing considerable errors in strain and temperature measurement. In this paper, we develop a new concept of two-end-access BOCDR, in which light is injected into each end of a sensing fiber in turn and the measured results of the Brillouin frequency shift distributions are combined. We numerically show that this configuration can suppress the systematic error caused by the AM-FM phase difference by approximately 90%.

Brillouin scattering in optical fibers has been a major tool for developing distributed strain and temperature sensors for several decades [1]. Such sensors are divided into two categories; one is two-end-access "analysis," which includes Brillouin optical time- [2, 3], frequency- [4], and correlation-domain [5, 6] analysis (BOTDA, BOFDA, and BOCDA). The other is single-end-access "reflectometry," which includes Brillouin optical time- [7], frequency- [8], and correlation-domain [9] reflectometry (BOTDR, BOFDR, and BOCDR). Combinations of some of these configurations have also been reported [10, 11]. Different configurations have different merits and demerits, but here let us focus on correlation-domain techniques, i.e., BOCDA and BOCDR, which have such advantages as relatively high spatial resolution and random accessibility to sensing points.

Although BOCDA and BOCDR utilize stimulated and spontaneous Brillouin scattering, respectively [12], they are both based on the same spatially resolving technique referred to as the synthesis of optical coherence functions (SOCF) [13,14]. In BOCDA and BOCDR, the optical frequency of the laser output is modulated to generate what we call a correlation peak (corresponding to a sensing point) in the fiber under test (FUT). By sweeping the modulation frequency, the position of the correlation peak can be scanned along the FUT, and the distributed information of the Brillouin gain spectrum (BGS) and/or the Brillouin frequency shift (BFS) can be obtained. In most of the BOCDA and BOCDR systems reported so far [15–23] (with a small number of exceptions [24–26]), a direct modulation scheme, in which the laser driving current was directly modulated to achieve optical frequency modulation (FM), was employed because of its simplicity and cost efficiency. However, the direct modulation scheme suffers from inevitable amplitude modulation (AM), which sometimes deteriorates the system performance such as spatial resolution [27,28].

In 2018, Song et al [29] reported a phenomenon where FM is delayed from AM by a phase difference $\Delta\varphi$ in the output of the modulated laser, resulting in the degraded measurement accuracy in BOCDA and BOCDR. When set to ±90°, the AM-FM phase difference has been reported to cause an error of up to tens of megahertz, which is systematic and cannot be suppressed by data averaging, while such an error does not exist when $\Delta\varphi$ is 0° or ±180°. To date, a new method using injection locking has been developed to compensate such errors in BOCDA [30]. However, no trial has been given to mitigate this error in BOCDR.

In this work, we propose a new concept of two-end-access BOCDR to suppress the systematic error caused by the AM-FM phase difference. Standard BOCDR operates by light injection to single end of the FUT, while in this configuration, the light is injected into each end of the FUT in turn to perform the same distributed BFS measurement in both directions and combine the obtained results to mitigate the error. Here, we numerically reveal the effect

of the two-end light injection. First, considering $\Delta\varphi$, we calculate the BGS and BFS distributions measured in standard single-end-access BOCDR and confirm that the results inevitably involve considerable errors. Subsequently, we calculate the combined BFS distributions measured in the new two-end-access BOCDR and show that the error caused by $\Delta\varphi$ can be suppressed by approximately 90%. Finally, we discuss this error compensation effect in the new configuration when intrinsic BFS is asymmetrically distributed outside the strained section, using an example where the applied strain is located near the fiber end.

The conceptual setup of standard BOCDR [9] is depicted in **Fig. 1(a)**. The optical output from a laser is divided into pump and reference light beams. The pump light is injected into an FUT, and the Stokes light is directed into a photo diode (PD). The reference light is used as an optical local oscillator. The electrical beat signal of the two light beams is monitored using an electrical spectrum analyzer (ESA). To resolve the position along the FUT, the optical frequency of the laser output is often modulated in a sinusoidal waveform by directly modulating the injection current of the laser (direct modulation scheme). From the viewpoint of temporal averaging, the coherence function is synthesized into a series of periodical peaks [13,14], the interval of which is in inverse proportion to the frequency of the sinusoidal modulation. We control the modulation frequency to generate only a single correlation peak within the range of the FUT. In a simple model, the peak frequency observed using the ESA gives the BFS caused at the specific position. By sweeping the modulation frequency, the position of the correlation peak is scanned along the FUT, and thus the BGS and BFS distributions can be obtained. The spatial resolution and the measurement range of standard BOCDR are given as Eqs. (15) and (16) in Ref. 12, respectively.

One of the most important merits of BOCDR lies in its operation capability by light injection into only one end of the FUT [9]. This single-end accessibility provides convenience in deployment, and in addition, the measurement can be continued even when the FUT is broken during operation. However, standard BOCDR suffers from the systematic error caused by the AM-FM phase difference, leading to considerable errors in strain and temperature measurement [29]. This is the reason why, at the cost of its single-end accessibility, we conceived a new concept of two-end access BOCDR, which can suppress the systematic errors by injecting light beams into both ends of the FUT and combining the obtained results. This method can be much more easily implemented than the injection-locking scheme in BOCDA [30]. Besides, it is more compatible with BOCDR than with BOCDA, because it is not easy to switch the pump and probe light beams with different frequencies in BOCDA.

To show the effectiveness of the two-end-access configuration, we calculated the BGS and BFS distributions, following the detailed analysis on the operation of standard BOCDR [12].

Here, we use two terms related to BGS: “intrinsic BGS” and “measured BGS.” The intrinsic BGS is the BGS at each position along the FUT, while the measured BGS is the BGS observed using BOCDR; the distributions of these two kinds of BGSs are different in principle. In BOCDR, the measured BGS distribution can be calculated using the intrinsic BGS distribution. More specifically, the measured BGS distribution is given by the square of the 2-dimensional convolution of the beat spectrum and the intrinsic BGS distribution [12]. The beat spectrum is defined as the power spectrum of the Fourier transformation of the cross-correlation between the reference light and the Stokes light.

The conceptual diagrams of the calculating process of the beat spectrum are shown in **Fig. 1(b)**. A time-domain method was used to calculate the beat spectrum to lower the complexity of the algorithm. First, an array was built to store the frequency values of the modulated reference light as time-dependent variables $f_0(t)$, followed by a matrix $f_B(t,x)$, which stores the frequency values of the Stokes light backscattered from each sampling point. The matrix for the beat signal frequency values was then obtained from the difference between the two as:

$$f_{\mathrm{beat}}(t,x) = f_0(t) - f_{\mathrm{B}}(t,x). \tag{1}$$

Subsequently, for each sampling point, the probability density function of the beat signal’s time-varying frequency falling within a certain frequency range was calculated by cumulating the number of sampling points within each frequency interval, converting the time-domain signal to the power spectrum, i.e., the beat spectrum. Finally, the intrinsic BGS distribution $g_{\mathrm{int}}(f,x_0)$ was created from an array storing the strain value of each position; it was defined as:

$$\begin{aligned} g_{int}(f,x_0) &= 0 \quad \text{when } f \neq f_{int} \\ \ldots\ldots\ldots\ldots\ldots &= 1 \quad \text{when } f = f_{int}, \end{aligned} \tag{2}$$

where f_{int} is the intrinsic BFS at position $x = x_0$, and was then 2-dimensinally convolved with the beat spectrum to produce the measured BGS distribution.

The conceptual setup of the two-end-access BOCDR system is shown in **Fig. 2**, in which light is injected into each end of the FUT in turn, controlled by an optical switch (OS). The system can be treated as standard single-end-access BOCDR each time light is injected into one end of the FUT. The eventual result is the simple arithmetic mean of the results obtained by performing distributed BGS and BFS measurements with light injected into each end of the FUT, which leads to the mitigated systematic errors.

In our calculation, a constant imaginary strain was applied to a certain area of the FUT to simulate the BFS change caused by an external effect in practical use (considering that the strain which is not constant within the spatial resolution cannot be accurately measured by

standard BOCDR, it is also unmeasurable in the two-end-access BOCDR). The length z of this area was expressed using a length unit R (nominal spatial resolution), which was calculated to be ~0.97 m by substituting the following parameters into Eq. (15) in Ref. 12: the Brillouin bandwidth $\Delta\nu_B$ = 30 MHz, the core refractive index n = 1.47, the modulation frequency f_m = 1 MHz, and the modulation amplitude Δf = 1 GHz. The AM employed was set to 9 dB, defined as the ratio of the maximum power to minimum. The phase of FM was delayed from that of AM by 90° ($\Delta\varphi$ = 90°) so that the worst $\Delta\varphi$ error was caused. The strain amplitude was set to cause a target BFS change ν_T of 50 MHz (corresponding to ~0.11% strain at 1550 nm) [31].

The measured and intrinsic BFS distributions in standard BOCDR and two-end-access BOCDR are shown in **Fig. 3(a)-(f)** (when z is (a,b) 2R, (c,d) 1.5R, and (e,f) R). Regardless of the strained length, the errors caused by $\Delta\varphi$ were clearly mitigated by two-end light injection. To give a quantitative comparison, we focused on the discontinuity point of the intrinsic BFS marked as x_0 and its neighborhood with a length of 2R (where the BFS distributions are most distorted in standard BOCDR), as shown in **Fig. 4**. We defined an error evaluation parameter Δh as

$$\Delta h = \Delta\nu - \nu_T\,, \tag{3}$$

where $\Delta\nu$ is the range of BFS values within the neighborhood of x_0, aiming to show the deviation between the measured BFS and the intrinsic BFS in the neighborhood of x_0.

The Δh values and the average values of the measured BFS within the strained section for standard and two-end-access BOCDR are shown in **Fig. 5(a)** and **5(b)**, respectively. The average values of the measured BFS were remained close to each other and floated around the target BFS of 10.90 GHz. However, regardless of the strained length z, the remarkable difference in Δh between the two configurations was obtained; for instance, at $z = R$, the absolute value of Δh in two-end-access BOCDR was smaller by 97% than that in standard BOCDR (at $z > 2R$, Δh in two-end-access BOCDR was smaller by >80%). Thus, the two-end-access configuration was shown to effectively compensate the measurement error caused by $\Delta\varphi$ in BOCDR.

However, as shown in **Fig. 6(a)** and **6(b)**, when the strain was applied near the fiber end (z was set to 2R), although the two-end-access BOCDR was still able to suppress the BFS dispersion, the average values of the measured BFS became 10.8974 GHz, being 2.6 MHz lower than the intrinsic BFS (10.90 GHz). This difference is much larger than that of the situation where strain is applied far from the fiber end (<1 MHz). A qualitative cause for such an error is the asymmetric distribution of the intrinsic BFS between the left and right of the strained section. When strain is applied near the fiber end, there are two discontinuity points

of the intrinsic BFS distribution at the positions of $x_1 = -2R$ and $x_2 = 0$. This situation can be regarded as one of the extreme cases of asymmetric distributions of the intrinsic BFS, which cause the asymmetric measured BFS distributions that cannot be compensated by two-end access configuration. This error caused by the asymmetric intrinsic BFS distributions may be compensated by some advanced signal processing, but further study is required on this point.

In conclusion, we proposed a new concept of two-end-access BOCDR to compensate the systematic error caused by the AM-FM phase difference in the light source. We showed that this configuration can effectively mitigate such systematic errors, except for the cases where the intrinsic BFS is asymmetrically distributed outside the strained section. Compared to the injection-locking technique previously reported for BOCDA [20], our method can be easily implemented and is more compatible with BOCDR than BOCDA. However, we need to admit that this configuration spoils one of the most important merits of BOCDR, i.e., single-end accessibility. It is true that the sampling rate will be less than half of that of standard BOCDR and that the random accessibility will be deteriorated. But these points may not be big issues, considering that some high-speed BOCDR configurations have been developed thus far [32–34]. We believe that, especially when measurement accuracy has more priority than single-end accessibility, two-end-access BOCDR with high simplicity will be one of the useful tools for distributed strain and temperature measurement in future.

Acknowledgments

This work was partly supported by the JSPS KAKENHI (17H04930, 17J07226, 20J22160, 21H04555) and research grants from the Noguchi Institute, the Murata Science Foundation, the Telecommunications Advancement Foundation, the Takahashi Industrial and Economic Research Foundation, and the Yazaki Memorial Foundation for Science and Technology.

References

1) A. Motil, A. Bergman, and M. Tur, Opt. Laser Technol. **78**, 81 (2016).
2) T. Horiguchi and M. Tateda, J. Lightwave Technol. **7**, 1170 (1989).
3) A. Denisov, M. A. Soto, and L. Thévenaz, Light: Sci. Appl. **5**, e16074 (2016).
4) D. Garus, K. Krebber, F. Schliep, and T. Gogolla, Opt. Lett. **21**, 1402 (1996).
5) K. Hotate and T. Hasegawa, IEICE Trans. Electron. **E83-C**, 405 (2000).
6) Y. H. Kim, K. Lee, and K. Y. Song, Opt. Express **23**, 33241 (2015).
7) T. Kurashima, T. Horiguchi, H. Izumita, S. Furukawa, and Y. Koyamada, IEICE Trans. Commun. **E76-B**, 382 (1993).

8) A. Minardo, R. Bernini, R. Ruiz-Lombera, J. Mirapeix, J. M. Lopez-Higuera, and L. Zeni, Opt. Express **24**, 29994 (2016).
9) Y. Mizuno, W. Zou, Z. He, and K. Hotate, Opt. Express **16**, 12148 (2008).
10) Y. Mizuno, Z. He, and K. Hotate, Opt. Express **17**, 9040 (2009).
11) D. Elooz, Y. Antman, N. Levanon, and A. Zadok, Opt. Express **22**, 6453 (2014).
12) Y. Mizuno, W. Zou, Z. He, and K. Hotate, J. Lightwave Technol. **28**, 3300 (2010).
13) K. Hotate and Z. He, J. Lightwave Technol. **24**, 2541 (2006).
14) K. Hotate, Appl. Sci. **9**, 187 (2019).
15) Y. Mizuno, Z. He, and K. Hotate, IEEE Photonics Technol. Lett. **21**, 474 (2009).
16) Y. Mizuno, Z. He, and K. Hotate, Opt. Express **18**, 5926 (2010).
17) N. Hayashi, Y. Mizuno, and K. Nakamura, J. Lightwave Technol. **32**, 3999 (2014).
18) Y. Okawa and K. Hotate, J. Opt. Soc. Am. B **37**, 2157 (2020).
19) B. Wang, Y. Dong, D. Ba, and X. Bao, Meas. Sci. Technol. **31**, 052001 (2020).
20) N. Hayashi, Y. Mizuno, K. Nakamura, C. Zhang, L. Jin, S. Y. Set, and S. Yamashita, Jpn. J. Appl. Phys. **59**, 088002 (2020).
21) Y. Mizuno, N. Motoishi, K. Noda, H. Lee, and K. Nakamura, Appl. Phys. Express **13**, 052001 (2020).
22) L. Zhao, Y. Wang, X. Hu, M. Zhang, J. Zhang, L. Qiao, T. Wang, S. Gao, and A. A. Himika, Opt. Express **28**, 18189 (2020).
23) Y. Mizuno, H. Lee, N. Hayashi, and K. Nakamura, Opt. Lett. **44**, 2097 (2019).
24) K. Noda, G. Han, H. Lee, Y. Mizuno, and K. Nakamura, Appl. Phys. Express **12**, 022005 (2019).
25) K. Noda, H. Lee, Y. Mizuno, and K. Nakamura, Jpn. J. Appl. Phys. **58**, 068004 (2019).
26) K. Noda, H. Lee, K. Nakamura, and Y. Mizuno, Appl. Phys. Express **13**, 082003 (2020).
27) K. Y. Song, Z. He, and K. Hotate, Opt. Express **14**, 4256 (2006).
28) K. Y. Song, Z. He, and K. Hotate, J. Lightwave Technol. **25**, 1238 (2007).
29) K. Song and J. Choi, Opt. Lett. **43**, 5078 (2018).
30) K. Y. Song, J. H. Youn and J. H. Choi, J. Lightwave Technol. **37**, 4421 (2019).
31) T. Horiguchi, T. Kurashima, and M. Tateda, IEEE Photonics Technol. Lett. **1**, 107 (1989).
32) Y. Mizuno, N. Hayashi, H. Fukuda, K. Y. Song, and K. Nakamura, Light: Sci. Appl. **5**, e16184 (2016).
33) H. Lee, N. Hayashi, Y. Mizuno, and K. Nakamura, IEEE Photon. J. **8**, 6802807 (2016).
34) H. Lee, K. Nakamura, and Y. Mizuno, Opt. Fiber Technol. **59**, 102312 (2020).

Figure Captions

Fig. 1. (a) Conceptual setup of standard BOCDR. ESA: electrical spectrum analyzer, FG: function generator, FUT: fiber under test, PD: photo diode. (b) Conceptual diagrams of the calculating process of the beat spectrum.

Fig. 2. Conceptual setup of two-end-access BOCDR using an optical switch (OS).

Fig. 3. Measured (black dotted curves) and intrinsic (red dashed lines) BFS distributions in standard BOCDR and two-end-access BOCDR when z was set to (a,b) $2R$, (c,d) $1.5R$, and (e,f) R.

Fig. 4. Definitions of the error evaluation parameters.

Fig. 5. Error evaluation parameters *vs.* strained length in standard BOCDR (blue circles) and two-end injection BOCDR (red triangles). (a) Δh and (b) average values of the measured BFS within the strained section.

Fig. 6. Measured (black dotted curves) and intrinsic (red dashed lines) BFS distributions in (a) standard BOCDR and (b) two-end-access BOCDR. Strain was applied near the fiber end ($z = 2R$).

Figures

Fig. 1.

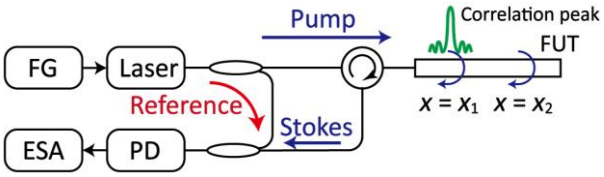

(a)

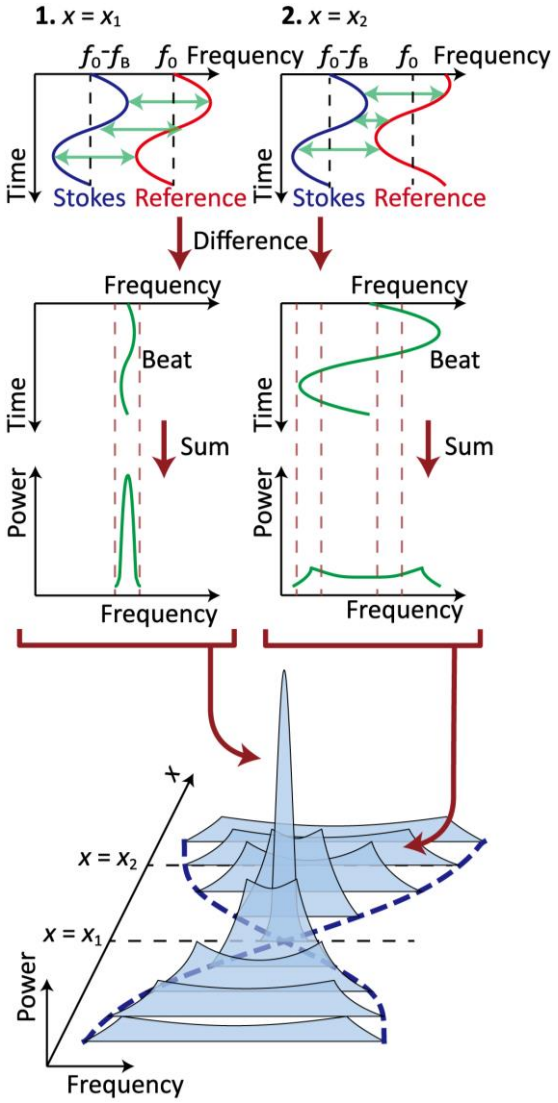

(b)

Fig. 2.

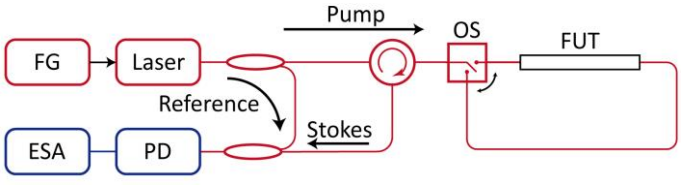

Fig. 3.

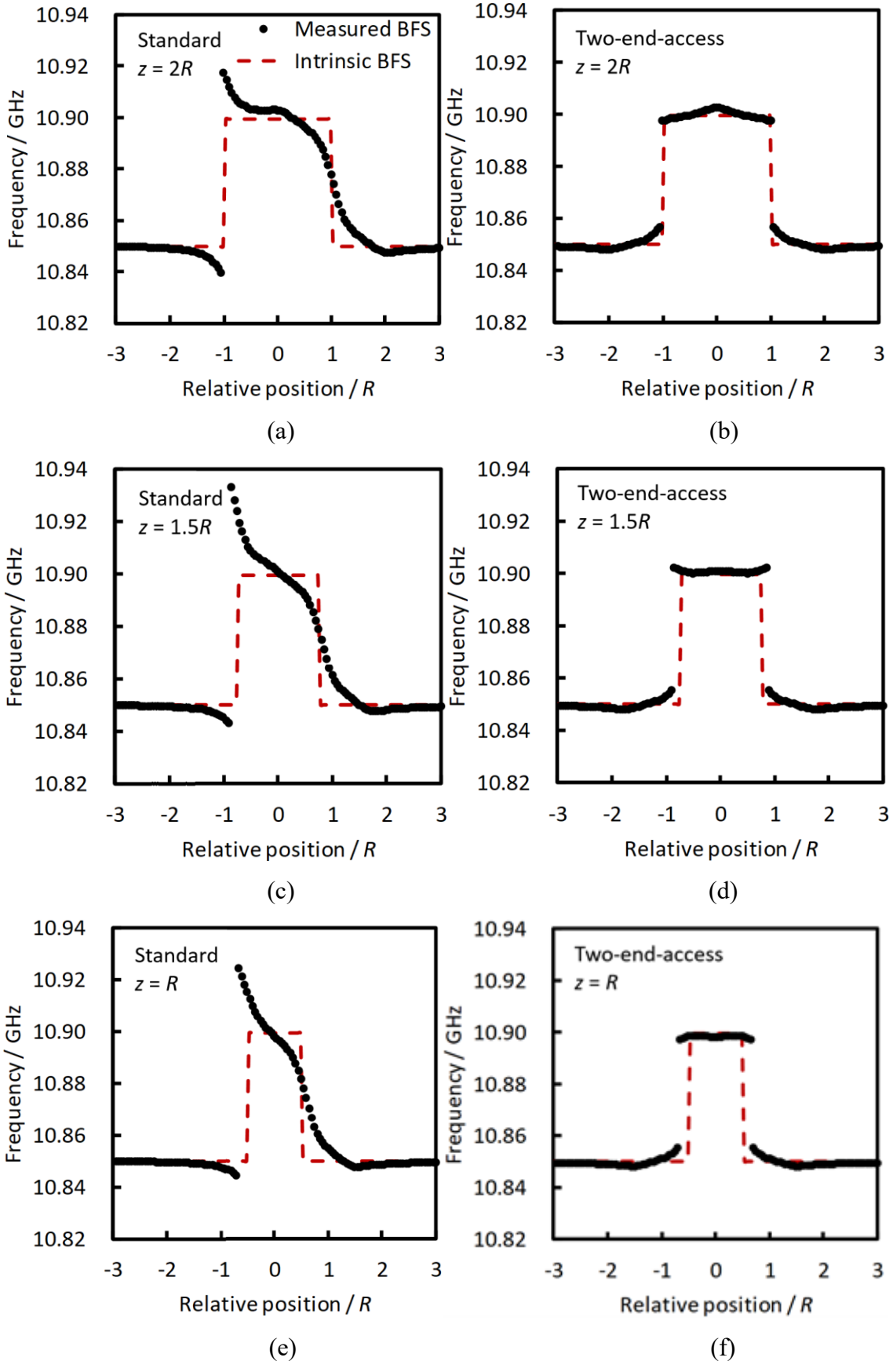
Standard
z = 2R
Measured BFS
Intrinsic BFS
Two-end-access
z = 2R
Standard
z = 1.5R
Two-end-access
z = 1.5R
Standard
z = R
Two-end-access
z = R
Frequency / GHz
Relative position / R
10.94
10.92
10.90
10.88
10.86
10.84
10.82
-3
-2
-1
0
1
2
3
(a)
(b)
(c)
(d)
(e)
(f)

Fig. 4.

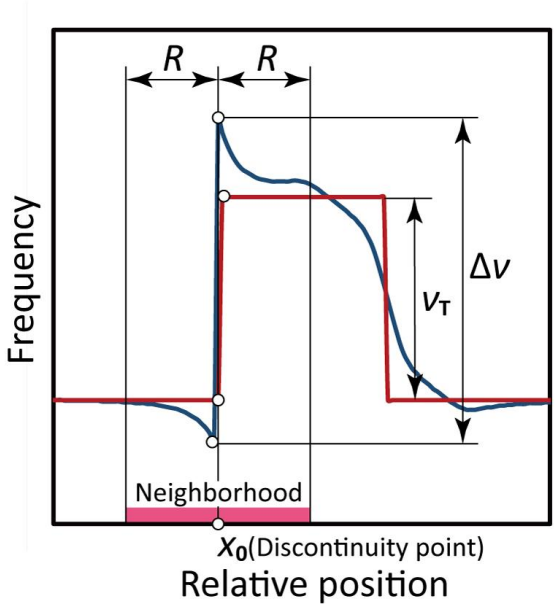
R
R
Frequency
Δv
v_T
Neighborhood
X_0(Discontinuity point)
Relative position

Fig. 5

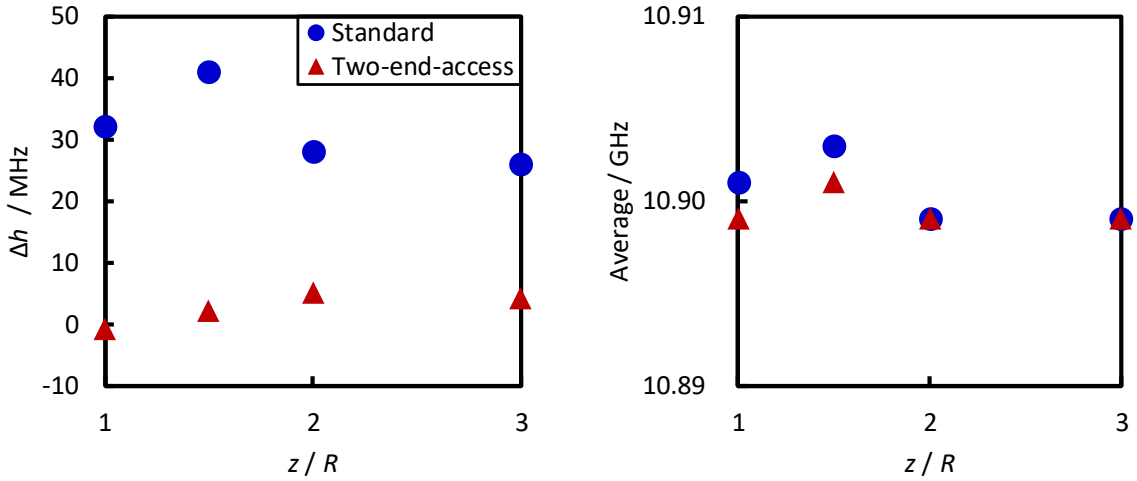
50
40
30
20
10
0
-10
Δh / MHz
Standard
Two-end-access
1
2
3
z / R
(a)
10.91
10.90
10.89
Average / GHz
1
2
3
z / R
(b)

Fig. 6

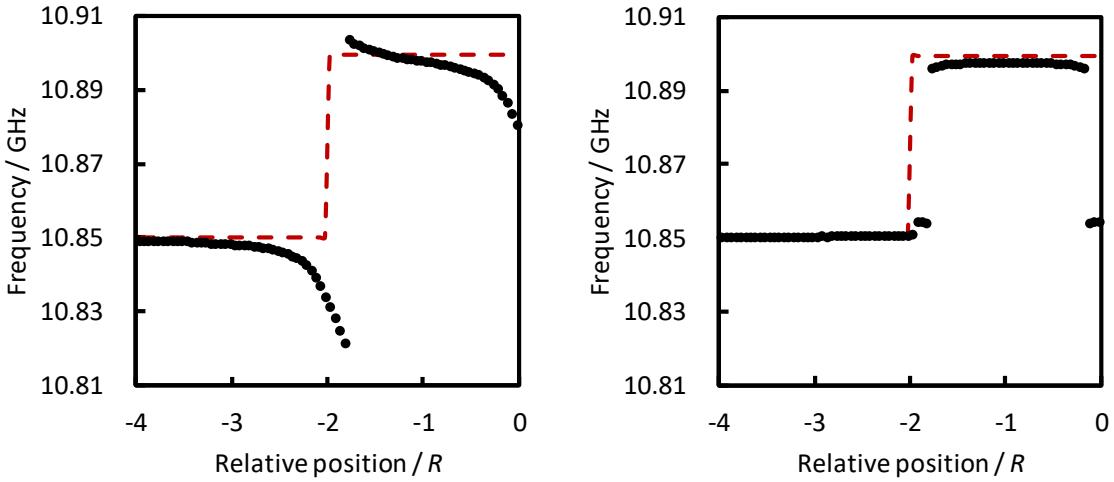
10.91
10.89
10.87
10.85
10.83
10.81
Frequency / GHz
-4
-3
-2
-1
0
Relative position / R
10.91
10.89
10.87
10.85
10.83
10.81
Frequency / GHz
-4
-3
-2
-1
0
Relative position / R

(a) (b)